

A NEW 1D METHOD FOR ASSESSING VOLUTE INDUCED CIRCUMFERENTIAL PRESSURE DISTORTION AT THE EXIT OF A CENTRIFUGAL IMPELLER

*T. Ceyrowsky**, *A. Hildebrandt**, *R. Schwarze*[†]

* Engineering Competence Center Aerodynamics, MAN Energy Solutions SE,
46145 Oberhausen, Germany

[†] Institute of Mechanics and Fluid Dynamics, Technical University Bergakademie Freiberg,
09599 Freiberg, Germany

Contact: thomas.ceyrowsky@man-es.com

ABSTRACT

Volute induced static pressure distortion may degrade impeller performance. In high-pressure applications, it can also severely affect mechanical operation. It is therefore worthwhile, to know the magnitude of pressure distortion at impeller exit. The authors present a detailed study of aerodynamic impeller-volute interaction. Firstly, CFD simulations of a volute stage are analysed: The distortion of radial velocity is a consequence of the volute's pressure field and remains almost constant throughout the vaneless diffuser. In contrast, at impeller exit, local discharge pressure determines tangential velocity, whereas towards diffuser exit, it is affected by the volute's pressure field. Aerodynamic blockage within the diffuser reduces static pressure at diffuser exit and hence mitigates absolute distortion. With these findings, a new 1D method for predicting the static pressure distortion at impeller exit is derived. Testing the model against CFD-results of further volute stages yields very good agreement at various operating conditions.

KEYWORDS

CENTRIFUGAL COMPRESSOR, VOLUTE, PRESSURE DISTORTION, VANELESS DIFFUSER, IMPELLER-VOLUTE INTERACTION

NOMENCLATURE

A	Area	[m ²]	p	Pressure	[Pa]	Δ	Difference	[-]
b	Width	[m]	u	Circumf. speed	[m/s]	ζ	Loss coefficient	[-]
Bl	Blockage	[-]	\dot{V}	Flowrate	[m ³ /s]	η	Isentr. Eff. $\eta = \frac{(p_{t\ out}/p_{t\ in})^{\kappa-1/\kappa-1}}{T_{t\ out}/T_{t\ in}^{-1}}$	[-]
c	Velocity	[m/s]	x	Variable	[-]	φ	Flow coefficient $\varphi = \frac{\dot{v}_{tot\ 0}}{\frac{\pi}{4}u_2d_2^2}$	[-]
c_p	Press. coeff.	[-]	z	Blade number	[-]	κ	Isentropic exponent	[-]
d	Diameter	[m]	α	Abs. flow angle*	[°]	θ	Circumferential angle	[°]
Ma	Mach number	[-]	β	Rel. flow angle*	[°]	ω	Loss coefficient	[-]

Subscript

2	Impeller exit	Des	Design condition	out	Stage outlet	up	Upstream of the tongue
4	Diffuser exit	dif	Diffuser	m	Mean	$down$	Downstream of the tongue
5	Volute exit	ef	Effective	rel	Relative	*	Related to tangent
av	Average	loc	Local	s	Static condition		
B	Blade	in	Stage inlet	tt	Total - total		

INTRODUCTION

If a centrifugal compressor's volute is operated at off-design conditions, flow is either de- or accelerated circumferentially, as has been explained in detail by Elholm et al. (1992) or Ayder et al. (1993). According to Bernoulli's law, this change of tangential velocity leads to a corresponding increase or decrease of static pressure. Especially in case of vaneless diffusers, any volute induced pressure distortion has a major impact on stage performance: First, the flow angle at volute inlet varies greatly, whereas a vaned diffuser aims at keeping flow angles constant. Since the inlet flow angle determines volute characteristics, both, the variance and the magnitude of pressure non-uniformity are much higher. Secondly, the static pressure distortion propagates through the vaneless diffuser towards the impeller. As several authors report, this pressure distortion is even noticeable at impeller inlet (e.g. Tamaki et al., 2012). In contrast, a vaned diffuser shields the impeller from the volute's pressure distortion (Jaatinen et al., 2009). However, the circumferential non-uniformity of static pressure has an unfavourable effect on diffuser- and impeller flow, which may deteriorate stage performance and stability (Yang et al., 2010). Accordingly, several recent publications aim at alleviating the consequences of volute induced non-uniformities on impeller flow (e.g. Zheng et al., 2014). Furthermore, pressure distortion causes additional radial forces, increasing the bearings' load and even being suspected to induce vibrations (Sorokes et al., 1998). While often negligible at atmospheric inlet conditions, in high-pressure applications the circumferential distribution of static pressure may be crucial for mechanical operation (Sorokes and Koch, 2000). However, there are only few publications addressing impeller-volute interaction. Sideris and Van den Braembussche (1986) experimentally investigated the effect of pressure distortion on impeller flow and developed a method for predicting velocity variations at impeller exit. Fatsis et al. (1995) carried out a numerical study with impellers with different blade exit angles. They showed that in case of backswept blades, the integration of static pressure at impeller exit gives a good approximation of the total radial force. Van den Braembussche et al. (1999) presented a deliberate model for impeller-volute interaction. They demonstrated that the static pressure field within the vaneless diffuser depends mainly on volute flow, whereas the impeller's reaction to local static pressure determines the circumferential distribution of total temperature, -pressure and flow angle. Recently, Ceyrowsky et al. (2018) carried out simulations of various impellers at different operating conditions. Their results reveal that whether pressure distortion is amplified or alleviated towards the impeller, depends on its blade exit angle, the level of Mach number and the amount of aerodynamic blockage within the vaneless diffuser.

This publication continues the work of Ceyrowsky et al. (2018). In the first part of the paper, two different stages are investigated by means of CFD. Initially, full stage calculations of one stage are carried out, to analyse the volute's impact. Thereby, a representative pressure distortion at diffuser exit is quantified. Furthermore, the fundamental cause of increasing volute losses towards smaller flowrates is identified. Then, the effect of aerodynamic blockage within the vaneless diffuser is analysed in detail, by comparing CFD-results of two different stages. Inspection of flow profiles in circumferential as well as in spanwise direction at different radii within the vaneless diffuser reveals the effect of pressure distortion on impeller- and diffuser flow. In the second part, a straightforward 1D-method for predicting the magnitude of static pressure distortion at impeller exit is derived. According to the CFD-analysis' findings, it is based on the impeller exit velocity triangles at different circumferential positions. As diffuser performance showed to have a notable effect on pressure distortion in CFD, it is also incorporated into 1D. Finally, this method is applied to various stages at different operating conditions and validated against CFD.

CFD ANALYSIS

Methodology

Analysed stages

Two stages, stage C and stage C_{FC} , are investigated in this part of the paper. Stage C_{FC} has a smaller design flowrate and is derived from stage C by adjusting the shroud contour to assure similar

aerodynamic conditions (flowcut derivative, see Figure 1). Both stages are designed particularly for this study and represent stages commonly used in industrial applications. Table 1 shows the respective design parameters. The intention for selecting these two impellers is the investigation of blockage effects: Although they feature the same 1D – velocity triangles, they differ in design flow coefficient. According to its higher span, stage C will exhibit higher Mach numbers at its shroud and increased secondary flows, leading to a more distorted flow profile at impeller exit and assumedly affecting vaneless diffuser flow and blockage.

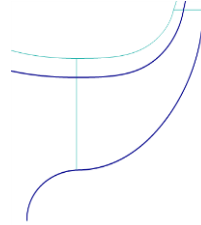


Figure 1: Meridional view of stage C (cyan) and its flowcut derivative C_{FC} (dark blue)

Table 1: 1D-parameters of analysed stages (angles relative to tangent)

	φ	u_2	β_{B2}	b_2/d_2	z	α_2	d_4/d_2	Ma_2	$A_5/(r_{5m} \cdot d_4)$
C	0.17	300 m/s	65°	8.3 %	15	32	1.5	0.65	0.19
C_{FC}	0.11			5.5 %					0.13

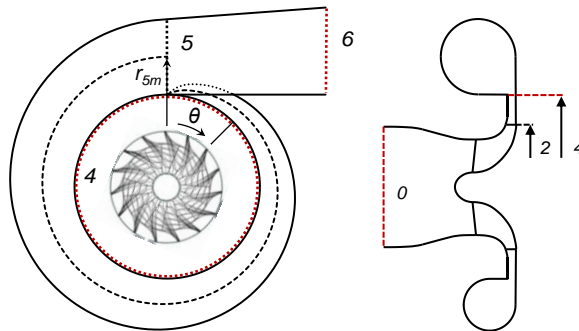


Figure 2: Nomenclature and computational domain

Numerical model

Steady state CFD analysis is carried out with NUMECA's commercial software. For the axially symmetric parts of the compressor, a block-structured grid is used (10 m cells), while the volute is resolved with an unstructured hexahedral mesh (7 m cells). Impeller and vaneless diffuser are modelled around the entire circumference. Rotating and stationary frame of reference are coupled with a frozen rotor interface. This method has been shown to be adequate for the present stage by Ceyrowsky et al. (2018), according to the acoustic Strouhal number criterion presented by Fatsis et al. (1995). A low-Reynolds k-epsilon model in the formulation of Yang and Shih (1993) is applied for turbulence closure. Further detailed information regarding mesh dependency and applicability of the frozen rotor method is available in Ceyrowsky et al. (2018). The entire CFD setup has been validated for a large number of representative test cases and is in accordance with MAN's best practice. Two different approaches are chosen for the current investigation. Firstly, full stage CFD calculations of stage C are carried out. The volute is included into the CFD model for estimating the magnitude of the pressure distortion it exerts and for analysing volute flow (see the computational domain in Figure 2). However, the motivation for the comparison of stages C and C_{FC} is to analyse the impact of blockage within the vaneless diffuser on the propagation of pressure distortion. Therefore, it is essential to apply exactly the same circumferential distortion profile at diffuser exit for both stages.

Accordingly, in the second approach, the volute is removed from the CFD model, and diffuser exit is set as domain outlet (section 4 in Figure 2). Initially, simulations with circumferentially uniform outlet conditions at diffuser exit are performed. Then, the volute-induced distribution of relative static pressure $p_{s\,loc}/p_s$, derived from stage C's full stage CFD calculations, is modelled by means of a half cosine wave with an amplitude of 10 %. Zheng et al. (2014) proved this method appropriate for simulating the volute's pressure distortion. It is chosen for it enables the application of comparable conditions at diffuser exit and it supersedes an additional, smaller volute for stage C_{FC}. For details regarding the modelled distortion, see Ceyrowsky et al. (2018).

Results

Analysis with volute

Figure 3 shows the circumferential distribution of relative static pressure of stage C at different radial positions. There is a distinct increase of circumferential static pressure at design flowrate. Despite properly matching, flow is decelerating within the external volute due to its design according to angular momentum. In contrast, at increased flow, static pressure is decreasing in circumferential direction. Pressure distortion at impeller- is lower than at diffuser-exit, especially at design flow. The profiles of relative radial velocity at impeller- and diffuser exit are almost congruent at 100- and 135 % flowrate (Figure 4). Only in the tongue region, there are slight differences: Since radial velocity is governed by pressure distribution, which is qualitatively equal at diffuser- and impeller exit, the profiles have the same shape at different radial positions. In Figure 5 at 100 % flowrate, tangential velocity decreases within the volute, while at diffuser exit its distribution is opposite: From a minimum at around 90°, tangential velocity increases in circumferential direction. At impeller exit, the profile resembles the one at diffuser exit, even if more uniform. Generally conflicting with the circumferential distributions of static pressure and radial velocity, tangential velocity differs at different radial positions: Within the volute, its development is determined by continuity. The resulting pressure distribution radiates towards impeller exit (see Figure 3), where local static pressure controls the individual passage's flowrate and defines the local velocity triangle, i.e. tangential velocity. Within the vaneless diffuser, it is determined by conservation of angular momentum. Approaching diffuser exit, flow is increasingly affected by the volute's pressure field and especially by the singularity of the tongue, as its potential field deflects flow and increases distortion of tangential velocity (see Figure 5). At highflow, there is only a moderate acceleration within the volute, since its high radius ratio of $r_{5m}/r_4 = 1.4$ prevents excessive acceleration. The corresponding circumferential decrease of static pressure results in a modest deceleration of tangential velocity at impeller exit. Again, at diffuser exit, its distribution is somewhat more pronounced, but still similar to that at impeller exit. In contrast to design flow, at high flow the distributions of tangential velocity within the volute and at diffuser exit are rather similar. Moderate differences arise only in the tongue region. In contrast, at design flow the profiles are twisted, revealing considerable differences of tangential velocities within volute and at diffuser exit.

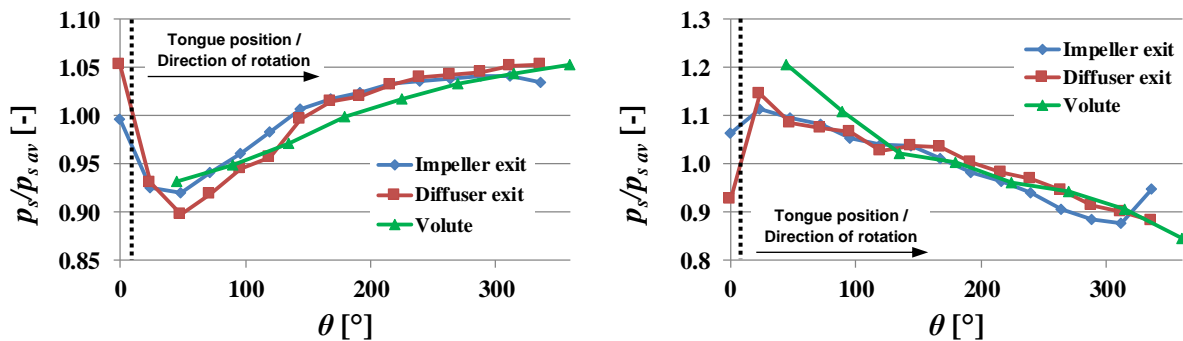


Figure 3: Relative static pressure @ 100 % (left) and 135 % flowrate (right)

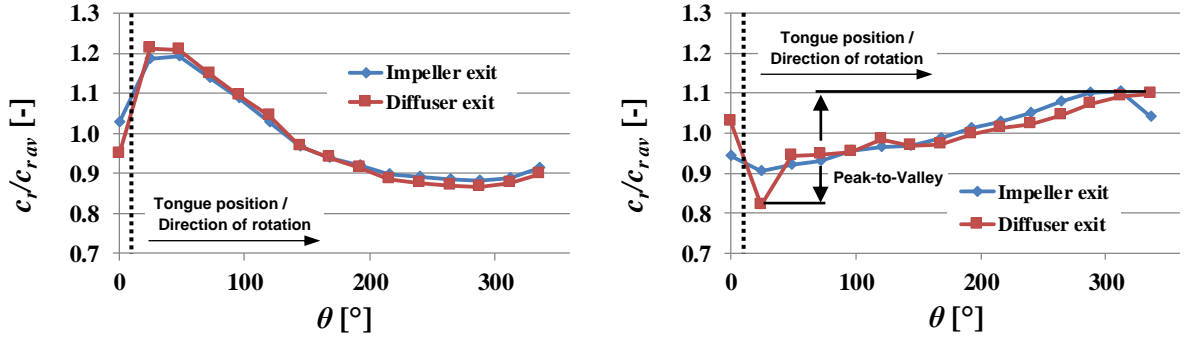


Figure 4: Relative radial velocity @ 100 % (left) and 135 % flowrate (right)

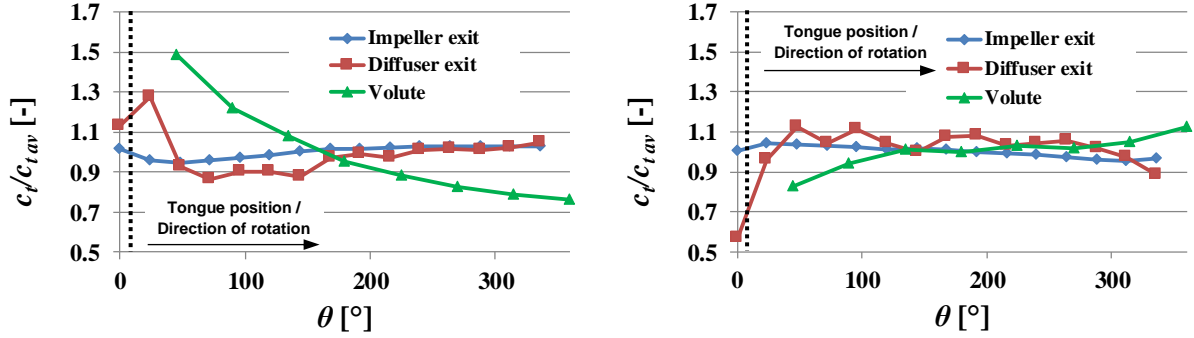


Figure 5: Relative tangential velocity @ 100 % (left) and 135 % flowrate (right)

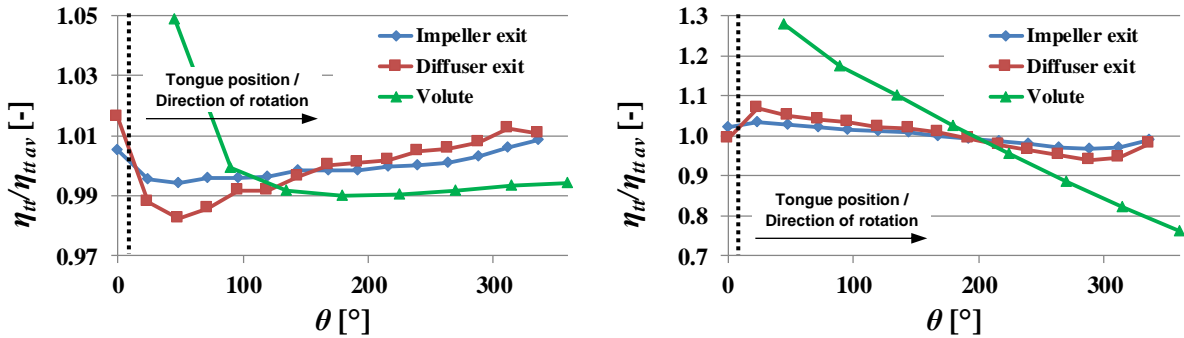


Figure 6: Relative isentropic efficiency @ 100 % (left) and 135 % flowrate (right)

Figure 6 shows the local isentropic efficiency related to the circumferentially averaged efficiency (within the volute, the average of the respective cross-section is related to the circumferential average). At 135 % flowrate, efficiencies at impeller- and diffuser exit decrease circumferentially in a similar manner, due to dethrottling. The volute strongly amplifies this trend. However, efficiency is still decreasing continuously. In contrast, at 100 % flowrate, the relative efficiency within the volute has a distinct maximum at 45°, followed by an abrupt drop towards 90°: In case of flow deceleration within the volute, losses arise primarily in the first quadrant, downstream of the tongue. As can be seen in Figure 5, fluid entering the volute here has been greatly accelerated. These high velocities lead to ineffective diffusion and excessive losses within the volute. This mechanism is visualised in Figure 7, showing the contours of the entropy gradient's magnitude at several circumferential positions within the volute at 100 % flowrate. While entropy accumulates along the flowpath, the magnitude of the entropy gradient increases only where entropy changes, and is therefore an immediate indicator for loss generation. Furthermore, at impeller- and diffuser exit, the local tangential velocity, related to the respective radial position's average value is plotted. While the circumferential distribution of tangential velocity at impeller exit is rather uniform, the local acceleration downstream of the tongue is clearly visible at diffuser exit. Accordingly, the magnitude

of the entropy gradient is maximum in the first two cross-sections downstream of the tongue. Further downstream, loss generation is modest and limited to the region of crossflow between diffuser exit and secondary vortex. This distribution of loss generation is in correspondence with the circumferential distribution of isentropic efficiency (Figure 6, left).

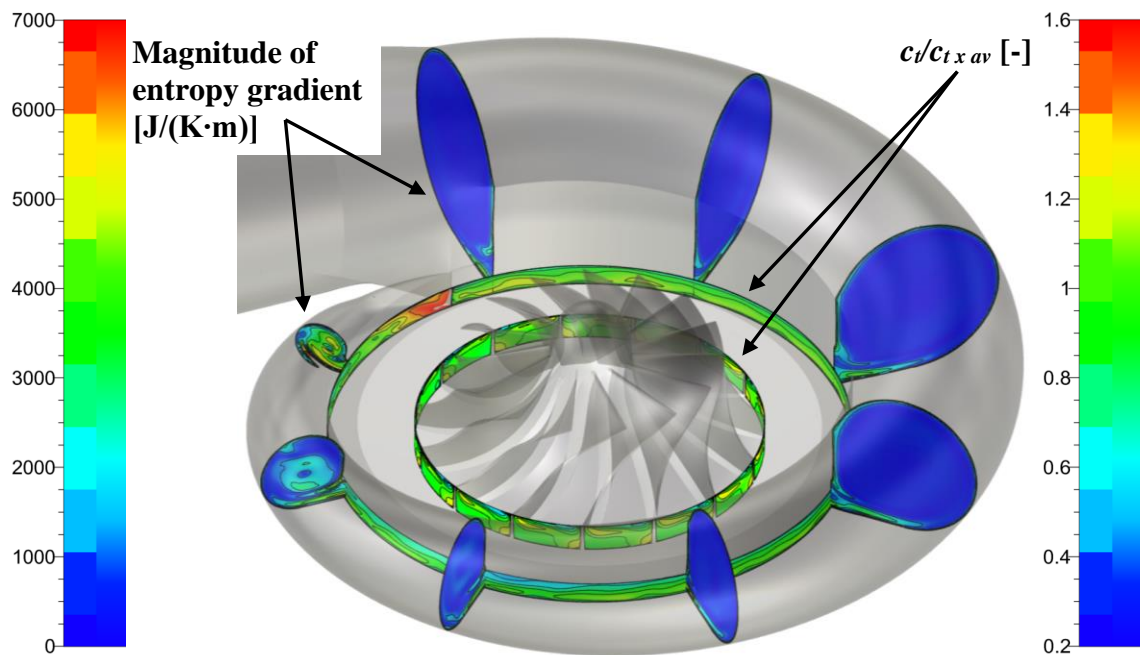


Figure 7: Magnitude of entropy gradient (volute) and relative tangential velocity (impeller- and diffuser exit) at 100 % flowrate

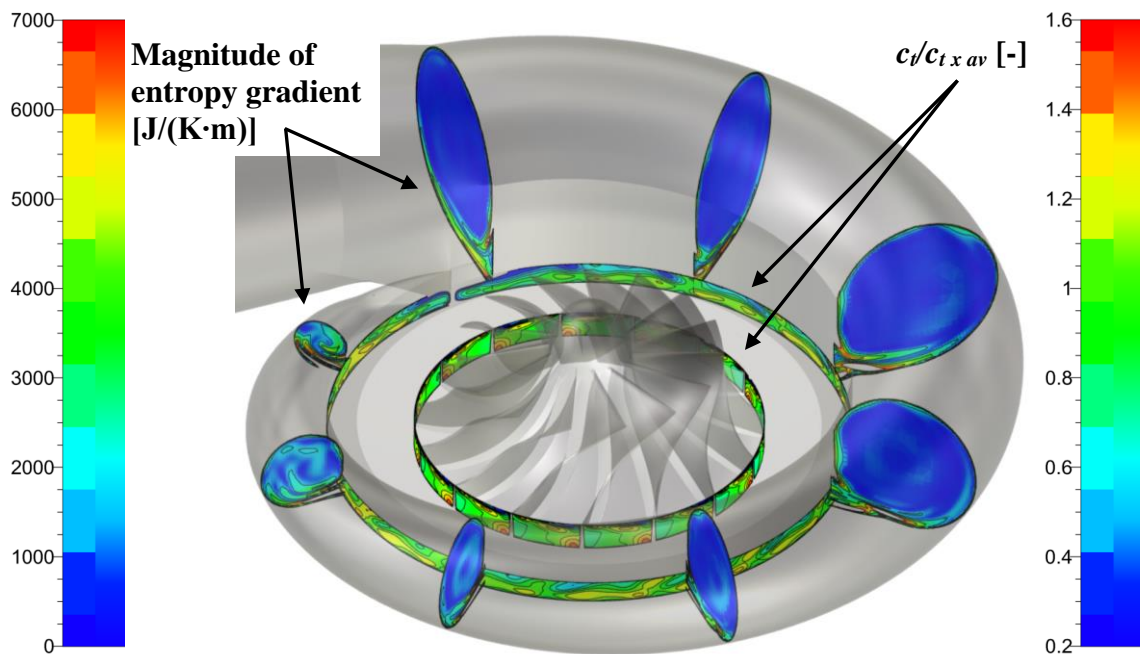


Figure 8: Magnitude of entropy gradient (volute) and relative tangential velocity (impeller- and diffuser exit) at 135 % flowrate

Figure 8 shows the same quantities at 135 % flowrate: At this operating point, there is no notable acceleration of tangential velocity around the tongue. Accordingly, the generation of losses is

distributed more even around circumference. Even in the three cross-sections upstream of the tongue there is a strong loss production in the crossflow region. Again, this distribution is consistent with the continuous circumferential decrease of efficiency within the volute (Figure 6, right). The effect of flow acceleration around the tongue is assumed one of the main sources of increasing volute losses in case of deceleration within the volute. The severity of this phenomenon strongly depends on the individual geometry, such as tongue design or transition from vaneless diffuser into the volute. Accordingly, this region is crucial for a successful volute design.

Analysis with modelled distortion

Figure 9 shows spanwise profiles of relative radial- and tangential velocity at a circumferential position opposite of the tongue, of stages C and C_{FC} at design point. At impeller exit, the radial- and tangential velocity profiles of stage C_{FC} are less distorted. However, according to its reduced absolute blade exit width, impeller C_{FC} 's tip vortex covers a broader portion of the channel. At diffuser exit, stage C's velocity profiles are even more distorted than at impeller exit. Again, the profiles of stage C_{FC} are more even at diffuser exit.

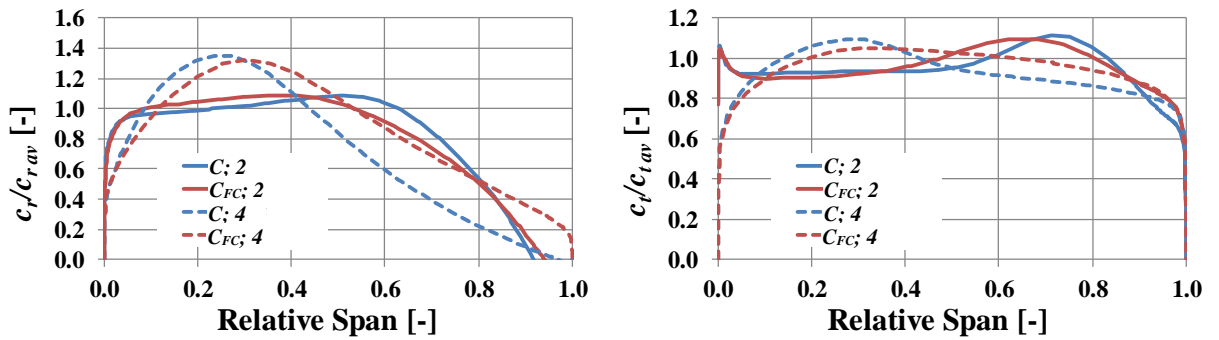


Figure 9: Spanwise profiles of relative radial (left) and tangential (right) velocities @ impeller- (2) and diffuser exit (4) of stages C and C_{FC} ; 0 → hub, 1 → shroud

Stronger distorted flow profiles correspond to an increased aerodynamic blockage Bl :

$$Bl = \frac{b - b_{ef}}{b}, \quad (1)$$

with the geometrical channel width b and the effective channel width $b_{ef} = \dot{V}/(c_r \cdot \pi \cdot d)$. According to continuity, increased blockage leads to higher meridional velocities. Figure 10 shows the aerodynamic blockage within the vaneless diffuser of stage C_{FC} related to that of stage C (left chart). While at impeller exit both stages exhibit a similar amount of blockage, towards diffuser exit ($d_4/d_2 = 1.5$), blockage of stage C_{FC} drastically reduces compared to that of stage C. Especially in the inner part of the vaneless diffuser ($1.00 < d/d_2 < 1.17$), flow diffuses much more efficiently. Accordingly, pressure recovery related to stage C increases notably. Only in the external part of the vaneless diffuser ($d/d_2 \geq 1.33$), relative pressure recovery decreases slightly, due to increasing losses of tangential velocity in stage C_{FC} 's diffuser, originating from its smaller hydraulic diameter. To understand the impact of diffuser performance on distortion propagation, circumferential peak-to-valley values (definition in Figure 4, right) of certain flow quantities of stages C_{FC} and C are related to each other:

$$\Delta x_{C_{FC}}/\Delta x_C = \frac{x_{\max C_{FC}} - x_{\min C_{FC}}}{x_{\max C} - x_{\min C}}, \quad (2)$$

where x is a variable for the individual quantity. If it exceeds unity, distortion of stage C_{FC} is higher than that of stage C. In the right chart in Figure 10, the corresponding ratios of static pressure, tangential-, radial- and absolute velocity within the vaneless diffuser are presented. Distortion of

radial velocity develops in inverse proportion to the blockage (left): Moving towards higher radii, blockage of stage C_{FC} reduces, while in contrast, its distortion of radial velocity is exceeding that of stage C: With reduced blockage, static pressure increases and average dynamic pressure reduces drastically. Due to this reduction of average dynamic pressure, its absolute circumferential differences have a bigger effect on the non-uniformity of radial velocity, even if distortion of static pressure reduces slightly. Considering tangential velocity, stage C_{FC} exhibits a slightly higher distortion at diffuser exit. The increased absolute static pressure distortion at the virtual tongue intensifies flow deflection. Between $1.16 < d/d_2 < 1.33$, differences between stages C_{FC} and C have almost vanished. At impeller exit, again, stage C_{FC} shows increased distortion of tangential velocity, due to the velocity triangle's stressed circumferential variation. Distortion of absolute velocity depends on the individual velocity component's non-uniformity, while tangential velocity has a somewhat bigger effect, since it is the major velocity component. Static pressure distortion throughout the vaneless diffuser is directly dependent on the absolute velocity's non-uniformity. Consequently, the ratios of pressure- and absolute velocity distortion are similarly shaped.

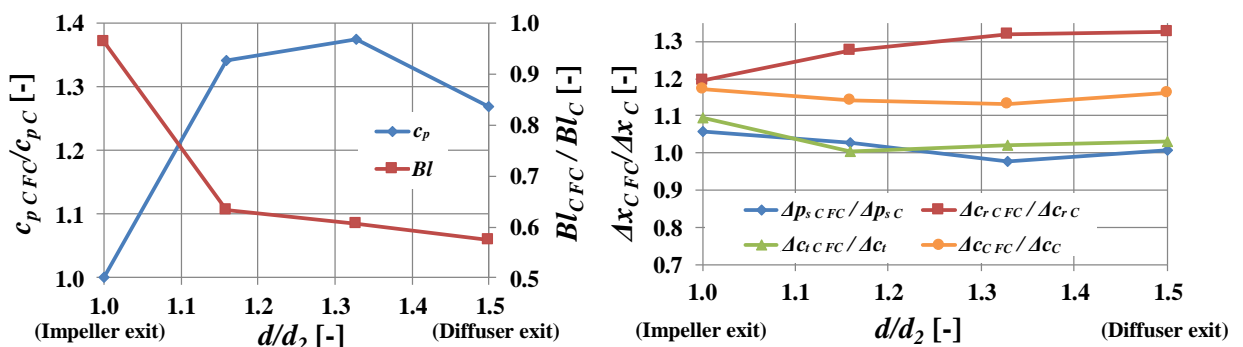


Figure 10: Pressure recovery and aerodynamic blockage (left) and distortion of pressure, radial- and tangential velocity (right) between stages C_{FC} and C within the vaneless diffuser

1D ANALYSIS

Fundamental model

The CFD-analysis reveals, that the propagation of non-uniformities from diffuser- to impeller exit is closely related to the development of the particular velocity components: The distortion of radial velocity is almost constant throughout the vaneless diffuser but its absolute level is affected by aerodynamic blockage. In contrast, tangential velocity is independent from blockage but its circumferential distribution varies within the diffuser: It is determined by the local velocity triangle at impeller exit and by the tongue's singularity at diffuser exit. According to the CFD-results, the following aspects are crucial for a 1D prediction of pressure distortion at impeller exit:

- The local velocity triangle at impeller exit (\rightarrow local passage throttling)
- The pressure recovery of the vaneless diffuser (\rightarrow diffuser blockage)
- The pressure difference between the tongue's pressure- and suction side (\rightarrow volute's pressure rise)

Any of the aforementioned effects can be considered in a classical 1D-calculation. However, the effort of this paper is to identify the effects, which are relevant for the propagation of pressure distortion, and to represent them with existing 1D methods. Therefore, only the equations relevant for following the approach are provided. Detailed information regarding 1D-calculation of impeller and vaneless diffuser flow is available in Eckert and Schnell (1961). The impeller is calculated by means of continuity and Euler equations, applying Wiesner's proven slip factor correlation, assuming a state of the art efficiency. Velocity components at vaneless diffuser exit are assessed, respecting

continuity of mass and conservation of angular momentum. Tangential velocity is charged with a simple assumption for friction. The discharge pressure at diffuser exit $p_{s\ 4\ av}$ is (Aungier (2000)):

$$p_{s\ 4\ av} = p_{s\ 2\ av} \cdot \left[1 + \frac{\eta_{dif} \cdot (T_{s\ 4\ av} - T_{s\ 2\ av})}{T_{s\ 2\ av}} \right]^{\frac{\kappa}{\kappa-1}}, \quad (3)$$

assuming a diffuser efficiency of $\eta_{dif} = 0.8$. The actual diffuser efficiency depends on several parameters such as relative diffuser width b_2/d_2 , flow profile at diffuser inlet, roughness and Reynolds Number. The chosen value is realistic for the given stage and may be adapted if necessary. Besides the individual velocity components, also total- and static temperature and pressure at impeller-, vaneless diffuser-, and volute exit are calculated. The results at impeller- and diffuser exit represent average conditions, as they occur in a passage opposite of the tongue. Then, the non-uniformity at diffuser exit is determined: Upstream of the tongue, static pressure $p_{s\ 4\ up}$ is set to match that at volute exit $p_{s\ 5}$. The assessment of volute flow relies on common assumptions for pressure recovery and losses. A detailed description is available in Ceyrowsky et al. (2018). The static pressure downstream of the tongue depends on the particular geometry and the transition from diffuser exit into the volute's first quadrant. In case of a notably cut back tongue, revision of equation (4) may be appropriate. In the present study, static pressure downstream of the tongue $p_{s\ 4\ down}$ is calculated as:

$$p_{s\ 4\ down} = p_{s\ 4\ av} \cdot \left(\frac{p_{s\ 4\ av}}{p_{s\ 5}} \right)^2. \quad (4)$$

$p_{s\ 4\ up}$ and $p_{s\ 4\ down}$ represent the backpressure for impeller- and diffuser passages next to the tongue and hence determine their operating points. Consequently, additional 1D-calculations are performed for these passages, where flowrate is adapted to match the respective static pressure at diffuser exit $p_{s\ 4\ up}$ and $p_{s\ 4\ down}$. The effect of throttling on the velocity triangle at impeller exit is intrinsically respected by the 1D-impeller calculation. Accordingly, tangential velocity, total pressure and total temperature at impeller exit are different for the three passages considered. However, the circumferential shift of total temperature and pressure within the diffuser is not considered. With the given absolute flow angle and the short diffuser, these quantities are transferred about only one impeller passage, which is negligible. In case of a lower flow angle or a longer diffuser, this effect may need to be taken into account. The effect of blockage on pressure recovery and consequently on distortion of radial velocity is considered by means of diffuser efficiency. Hence, static pressures at the particular impeller passages' exit represent the expected pressure distortion:

$$\Delta p_{s\ rel\ 2} = \left| \frac{p_{s\ 2\ up} - p_{s\ 2\ down}}{p_{s\ 2\ av}} \right|. \quad (5)$$

Analysed stages and methodology

The method described above is applied to stage C and to two additional unshrouded compressor stages, A and B. Table 2 gives an overview of their individual design parameters. With these stages, the 1D-method's sensitivity to particular parameters, known to affect distortion propagation, is examined: All stages have different Mach numbers at diffuser exit, stages A and C differ in blade exit angle and stages A and B feature different diffuser ratios.

Three different approaches are tested at design point of stage C: First, any passage's impeller efficiency is adjusted according to CFD, with circumferentially constant diffuser efficiency. Then, impeller efficiency is kept constant, while diffuser efficiency is adapted to CFD for passages down, av and up. Finally, both components' efficiencies are held constant in circumferential direction. The respective efficiencies are shown in Table 3. Subsequently, all three stages are investigated according to the 3rd approach, at three additional operating points: Low flow ($\varphi/\varphi_{Des} = 0.85$) and overload

($\varphi/\varphi_{Des} = 1.25$) at design speed, and design flow at an increased circumferential speed of $u_2 = 420 \text{ m/s}$. The method is validated against CFD-results, at any operating point. The numerical setup is the same as described earlier, with the volute included into the CFD model (full stage calculations).

Table 2: 1D-design parameters of stages A, B and C

	$u_{2 \text{ des}}$	α_2	z	β_{B2}	φ	b_2/d_2	d_4/d_2	Ma_2	Ma_4
A	300 m/s	32°	15	40°	0.12	8.3 %	1.50	0.50	0.34
B				40°	0.14	9.6 %	1.75	0.50	0.28
C				65°	0.17	8.3 %	1.50	0.65	0.43

Table 3: Different assumptions of component efficiencies

Approach	1	2	3
$\eta_{Impeller}$ [-] (down / av / up)	0.951 / 0.954 / 0.958	0.92	0.92
$\eta_{Diffuser}$ [-] (down / av / up)	0.8	0.48 / 0.80 / 0.80	0.80

Results

Impact of circumferential efficiency variations

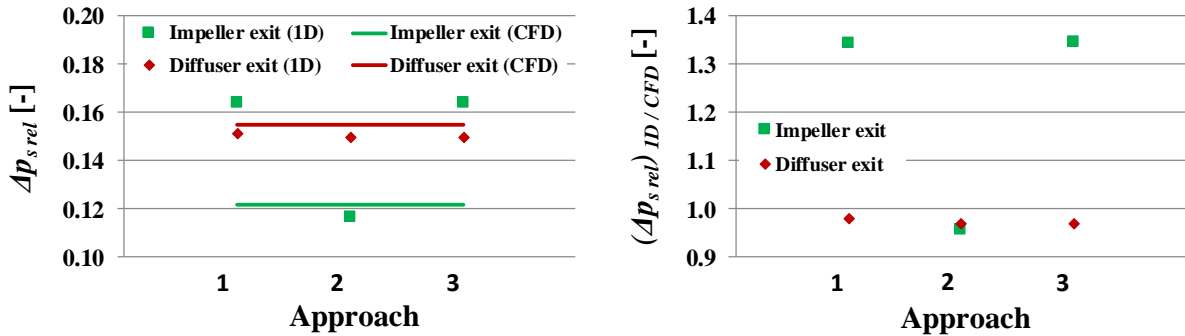


Figure 11: 1D- and CFD predicted pressure distortion at impeller- and diffuser exit (left); Ratio of 1D- and CFD predicted pressure distortion (right)

Figure 11 shows the relative pressure distortion at diffuser- and impeller exit, calculated by 1D and CFD (left) and the respective deviations (right). CFD predicts a distortion of 15.5 % at diffuser exit (equation (5)), while 1D yields 15.2 % with approach 1 (adjusted impeller efficiency) and 15.0 % with approaches 2 and 3 (constant impeller efficiency). This relates to a deviation of 2.1 % (approach 1) and 3.2 % (approaches 2 and 3), respectively. Apparently, the modest circumferential variations in impeller efficiency have a minor impact. At impeller exit, approach 2 (adjusted diffuser efficiency) somewhat underestimates distortion by 4.5 %. In contrast, approaches 1 and 3 (constant diffuser efficiency) notably overestimate pressure distortion, by about 34 %: Due to its high flow coefficient and blade exit angle (see Table 2), the impeller C has a distorted outlet flow profile. Hence, diffuser flow is more sensitive to local discharge conditions and prone to separations. Neglecting the notable circumferential differences in diffuser efficiency (see Table 3), causes a certain loss of accuracy. However, in case of more uniform diffuser performance, deviations will diminish. Finally, the results of approach 3 are in the correct order of magnitude and conservative, as distortion is overestimated.

Investigation of different operating points

Figure 12 presents the results of the different stages and operating points, predicted by 1D according to approach 3 and CFD. At diffuser exit (left), trends between the particular operating

points are well captured by 1D. In case of all stages, pressure distortion at diffuser exit is lowest at high flow and increases with further throttling. Only in case of stage C, 1D is predicting a marginally further increase of non-uniformity. For all stages maximum distortion is predicted for design flow at increased speed $u_2 = 420 \text{ m/s}$, concordantly by 1D and CFD. Also regarding the differences between the individual stages, 1D agrees very well with CFD: Regardless of the operating point, stage C generates the highest pressure distortion, followed well spaced out by stages A and B. At impeller exit, the differences between 1D and CFD are bigger. However, the trends between the different operating points and stages are predicted consistently, just like at diffuser exit. The order of magnitude of the 1D predicted pressure distortion agrees well with CFD. In case of any stage, 1D overestimates pressure distortion, except at high flow for stages A and B, where deviations have almost vanished.

For improving accuracy, firstly the prediction of volute losses is one key factor, as the volute's pressure recovery causes distortion at diffuser exit. Regarding stage A, the discrepancies at impeller exit are actually caused by an overestimation of pressure recovery within the volute. Another aspect, especially in case of highly loaded impellers like stage C, is the use of a non-uniform diffuser efficiency. This would notably enhance the 1D prediction. However, in case of stages A and B, despite the assumption of uniform diffuser efficiency, pressure distortion is well predicted.

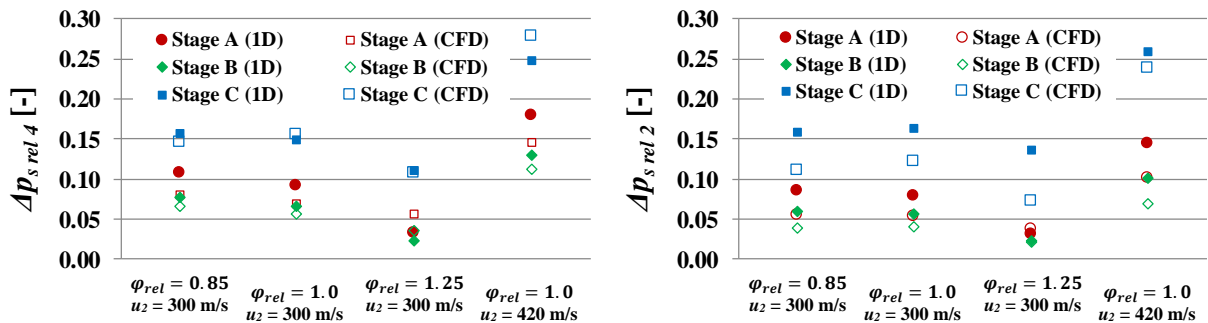


Figure 12: 1D- and CFD predicted pressure distortion at different operating points for stages A, B and C at diffuser- (left) and impeller exit (right)

CONCLUSIONS

In this work, a thorough investigation on impeller – volute interaction of centrifugal compressors with vaneless diffusers is presented. First, steady state CFD calculations are analysed in detail. Based on these findings, a straightforward 1D method for the prediction of static pressure distortion at impeller exit is presented. These are the main conclusions:

- While the circumferential distribution of radial velocity is almost constant throughout the diffuser, tangential velocity's distortion is changing: At impeller exit, it is defined by the local velocity triangle whereas at diffuser exit, it is affected by the tongue's pressure distribution.
- If tangential velocity is decreasing within the volute, it increases circumferentially at diffuser exit. The reason is flow deflection from the tongue's pressure to its suction side. The resulting deceleration downstream of the tongue generates high losses and can be considered one of the main reasons for decreasing performance of too big volutes.
- Aerodynamic blockage within the vaneless diffuser increases average dynamic pressure at diffuser exit. Accordingly, the relative circumferential differences in dynamic pressure reduce, resulting in a lower distortion of radial velocity.
- A 1D calculation of three representative passages is capable of predicting the pressure distortion at the exit of the impeller. While circumferential differences in impeller passage efficiency are negligible, the respective diffuser efficiency has a stronger impact on accuracy. In addition, the prediction of volute losses is crucial.

- The relations between different operating points and stages are well represented by 1D. Even with the assumption of circumferentially uniform impeller- and diffuser performance, predicted distortion at impeller exit is still in the correct order of magnitude and, as distortion is overestimated, deviations are conservative.

ACKNOWLEDGEMENTS

The authors wish to thank MAN Energy Solutions SE for the support of this study and the permission to publish the results.

REFERENCES

- Aungier, R. (2000). *Centrifugal Compressors*. ASME Press New York, 2000
- Ayder, E., V. d. Braembussche, R., Brasz, J. J., (1993). *Experimental and Theoretical Analysis of the Flow in a Centrifugal Compressor Volute*. Journal of Turbomachinery, Vol. 115: 582 – 589, 1993
- Ceyrowsky, T., Hildebrandt, A., Schwarze, R., (2018). *Numerical investigation of the circumferential pressure distortion induced by a centrifugal compressor's external volute* (GT2018-75919). Proceedings of ASME Turbo Expo 2018, Lillestrøm, Norway, 2018
- Eckert, B., Schnell, E., (1961). *Axial- und Radialkompressoren*. Springer Verlag Berlin / Göttingen / Heidelberg, 1961
- Elholm, T., Ayder, E., Van den Braembussche, R. A., (1992). *Experimental Study of the Swirling Flow in the Volute of a Centrifugal Pump*. Journal of Turbomachinery, Vol. 114: 366 – 372, 1992
- Fatsis, A., Pierret, S., Van den Braembussche, R. A., (1995). *3D unsteady flow and forces in centrifugal impellers with circumferential distortion of the outlet static pressure* (95-GT-33). Proceedings of ASME Turbo Expo 1995, Houston, Texas, USA, 1995
- Jaatinen, A., Backman, J. L. H., Turunen-Saaresti, T., (2009). *Radial forces in a centrifugal compressor equipped with vaned diffusers* (GT2009-60130). Proceedings of ASME Turbo Expo 2009, Orlando, Florida, USA, 2009
- Sideris, M. T., Van den Braembussche, R. A., (1986). *Influence of a Circumferential Exit Pressure Distortion on the Flow in an Impeller and Diffuser* (86-GT-9). Proceedings of ASME Turbo Expo 1986, Düsseldorf, Germany, 1986
- Sorokes, J. M., Borer, C. J., Koch, J. M., (1998). *Investigation of the Circumferential Static Pressure Non-Uniformity caused by a Centrifugal Compressor Discharge Volute* (98-GT-326). Proceedings of ASME Turbo Expo 1998, Stockholm, Sweden, 1998
- Sorokes, J. M., Koch, J. M., (2000). *The influence of low solidity vaned diffusers on the static pressure non-uniformity caused by a centrifugal compressor discharge volute* (GT2000-454). Proceedings of ASME Turbo Expo 2000, Munich, Germany, 2000
- Tamaki, H., Zheng, X., Zhang, Y., (2012). *Experimental investigation of high pressure ratio centrifugal compressor with axisymmetric and non-axisymmetric recirculation device* (GT2012-68219). Proceedings of ASME Turbo Expo 2012, Copenhagen, Denmark, 2012
- Van den Braembussche, R. A., Ayder, E., Hagelstein, D., Rautenberg, M., Keiper, R., (1999). *Improved Model for the Design and Analysis of Centrifugal Compressor Volutes*. Journal of Turbomachinery, Vol. 121: 619 – 625, 1999.
- Yang, Z., Shih, T. H., (1993). *New time-scale based k-epsilon model for near wall turbulence*. AIAA Journal , Vol. 31, No. 7: 1191 – 1198, 1993
- Yang, M., Zheng, X., Zhang, Y., Bamba, T., Tamaki, H., Huenteler, J., Li, Z., (2010). *Stability improvement of high-pressure-ratio turbocharger centrifugal compressor by asymmetric flow control – part I: Non-axisymmetric flow in centrifugal compressor* (GT2010-22581). Proceedings of ASME Turbo Expo 2010, Glasgow, United Kingdom, 2010
- Zheng, X., Lei, J., Tamaki, H., (2014). *Influence of volute-induced distortion on the performance of a high-pressure-ratio centrifugal compressor with a vaneless diffuser for turbocharger applications*. Proceedings of the Institution of Mechanical Engineers, Part A: Journal of Power and Energy, Vol. 228: 440 - 450, 2014